J. Alloys and Compounds 930 (2023) 167381 1D
https://doi.org/10.1016/j.jallcom.2022.167381

On the order of magnetic transition in $MnCo_{1-x}Fe_xGe$ (x = 0.20, 0.06 and 0.03) mechanical alloys

A. Vidal-Crespo, J.J. Ipus*, J.S. Blázquez, C.F. Conde

Departamento Física de la Materia Condensada, ICMSE-CSIC, Universidad de Sevilla, P.O. Box 1065, 41080 Sevilla, Spain

Corresponding author email: jhonipus@us.es

Abstract

Mechanically amorphized $MnCo_{1-x}Fe_xGe$ alloys (x = 0.20, 0.06 and 0.03) were used as precursors to obtain hexagonal austenite single phase samples. Combining thermomagnetic and magnetocaloric analysis and in situ X-ray diffraction, we observed that the presence of a distribution of transition temperatures jeopardizes the first order character of the magnetoelastic transition from the ferromagnetic to paramagnetic state. Both magnetothermal and in situ X-ray diffraction identify the presence of such distribution and the first order character of the magnetoelastic transition.

Keywords: mechanical alloying, order transition, magnetocaloric effect, magnetoelastic transition

1. Introduction

There is an important awareness in our society to reduce the energetic consumption. To achieve this goal is necessary to develop new technological applications, among which magnetic refrigeration based on the magnetocaloric effect (MCE) could be an excellent candidate for its high efficiency compared to conventional refrigeration systems [1]. In this sense, it is desirable to obtain materials that show large MCE around room temperature in the context of domestic applications. MCE consists in the heating or cooling of a magnetic material when a magnetic field is applied or removed [2]. To indirectly characterize this phenomenon, the magnetic entropy change, ΔS_M, can be used, which is related to the temperature change of magnetization, M, by the Maxwell relation.

$$\Delta S_M = \mu_0 \int_0^{H_{max}} \left(\frac{\partial M}{\partial T}\right)_H dH \quad (1)$$

Where μ_0 is the permeability of vacuum, H is the magnetic field and T is the temperature. When the specific magnetization, σ, is used the entropy change per unit mass is obtained. From this equation, it is deduced that the MCE is maximum around a phase transition (high variation in M). Transitions can be classified into two categories: first (FOPT) or second order (SOPT) character, attending to the order of the derivative of energy to be discontinuous. On the one hand, FOPT materials are characterized by a larger MCE

response than those with SOPT but with significant values restricted to a smaller temperature range and, generally, affected by hysteresis. On the other hand, although SOPT materials show smaller ΔS_M peaks than the FOPT materials, significant values extend to a wider temperature range whereas thermal hysteresis are absent and magnetic hysteresis can be negligible in soft magnetic materials.

In the present study we focus on martensitic alloys, which magnetic transitions are very interesting for their MCE [3–9] due to the coupling between structure and magnetism during the transition. In particular, this work deals with MnCoGe intermetallic compounds where Fe partially substitutes for Co and produced by low temperature annealing of mechanically alloyed amorphous precursors. It is worth noticing that conventional production process of these alloys leads to samples with a reversible transformation at about 420 K from a martensitic orthorhombic phase (TiNiSi type structure with a space group $Pnma$) to an austenitic hexagonal phase (Ni_2In-type structure with a space group $P6_3/mmc$)[10]. For MnCoGe, the Curie temperatures of hexagonal austenite and orthorhombic martensite are 276 K and 355 K, respectively [11]. As a result, the martensite transformation occurs in the paramagnetic state, which is not relevant to MCE. However, the magnetostructural martensitic transformation can be tuned to overlap with Curie temperature of both phases by applying physical pressure or chemical modifications [12–14], so that FOPT can be found around room temperature. In particular, partial substitution of Fe for Co can be a good compositional change to improve MCE [14]. However, the formation of the intermetallic phase of interest is not simple and thermal treatments at high temperatures for long times are needed [15–17], which can be overcome by using precursor systems produced by mechanical alloying [18]. Through this technique, micrometric powder particles are obtained, with crystallite size in the order of 10 nanometers, or even with amorphous structure. The homogeneity of such precursors can reduce both the temperature and the annealing time needed to produce the intermetallic phase of interest from them [19].

In this work, the characteristics of the magnetic transition in $MnCo_{1-x}Fe_xGe$ (x = 0.20, 0.06 and 0.03) series are analyzed taking into account the presence of a distribution of transition temperatures and in situ microstructural measurements. The field exponent of ΔS_M, n, and its dependency on the nature of the transition order as well as the existence of the mentioned Curie temperature distribution were studied and related to the in-situ evolution of the cell volume as a function of temperature.

2. Experimental

Production of $MnCo_{1-x}Fe_xGe$ (in at. %) alloys, with x = 0.20, 0.06 and 0.03 follows the same steps as in [19,20]. First, a mixture of powders (purity >99 %) was milled in Ar atmosphere in a Fritsch Pulverisette Vario 4 planetary mill in order to produce homogeneous precursors (10 mm diameter steel balls; 80 cm^3 hardened steel vials; ball to powder mass ratio 10:1; ratio between rotational speeds of vials and main disk −2). Second, samples were heated up to 723 K to develop the intermetallic phase.

Chemical composition was performed by X-ray fluorescence, XRF, (EAGLE III) and microstructure characterization by X-ray diffraction, XRD, (D8 Advance A25 diffractometer at room temperature and Bruker D8C diffractometer for controlled temperature and atmosphere experiments, Cu-K_α radiation in both). X-ray analysis software used was 4.1 Bruker DIFFRAC.EVA (phase identification) and 6.0 Bruker DIFFRAC.TOPAS (Rietveld refinement). Thermal treatments were performed in a DSC7 Perkin-Elmer calorimeter operating in Ar flow at a heating rate of 20 K/min. A Lakeshore 7407 Vibrating Sample Magnetometer, VSM, was used to study field and temperature dependence of magnetization (maximum applied field 1.5 T with a sweep rate of ~1.5 K/min). For these measurements, as-milled powders were compacted at room temperature at 2 tons in 5 mm disks of < 0.5 mm high. A piece of these disks (< 3 mm) was placed in the magnetometer rod aligned with the magnetic field parallel to the surface of the disk. Magnetic entropy change was calculated from isothermal magnetization curves applying the Maxwell relation, described in Eq. 1, with the help of Magnetocaloric Effect Analysis program [21].

3. Results

The chemical composition of 100 h milled sample with x = 0.20 can be found in [19]. For the other two samples, the general behavior is the same concerning Ge and transition metals content (ascribed to brittle character of Ge and ductile one of the transition metals). This leads to slight deviations with respect to the nominal composition, as shown in **Table 1**. However, in the following we will refer to the nominal composition for simplification.

Table 1. Composition observed by X-ray microfluorescence ($MnCo_{1-x}Fe_xGe$) after 50 h

x = 0.20			x = 0.06			x = 0.03		
Element	**At. % expected**	**At. % observed**	**Element**	**At. % expected**	**At. % observed**	**Element**	**At. % expected**	**At. % observed**
Mn	33.33	30.8 ± 0.2	Mn	33.33	32.9 ± 0.1	Mn	33.33	33.5 ± 0.2
Co	26.67	25.0 ± 0.2	Co	31.33	27.8 ± 0.2	Co	32.33	29.5 ± 0.2
Fe	6.67	7.0 ± 0.1	Fe	2.00	4.3 ± 0.4	Fe	1.00	2.4 ± 0.6
Ge	33.33	37.2 ± 0.3	Ge	33.33	35.0 ± 0.2	Ge	33.33	34.7 ± 0.5
$Mn_{0.92}Co_{0.75}Fe_{0.21}Ge_{1.12}$			$Mn_{0.99}Co_{0.83}Fe_{0.13}Ge_{1.05}$			$Mn_{1.00}Co_{0.88}Fe_{0.07}Ge_{1.04}$		

Fig. 1 shows the room temperature XRD patterns of as-milled samples after two milling times. A more complete evolution with milling time for the sample with x = 0.20 can be found in [19]. In all the cases, an amorphous halo is formed as milling progresses beyond 30 h. After 50 h milling, a recrystallization process is detected which leads to the formation of the intermetallic phase of interest in this study ($P6_3/mmc$ space group). This recrystallization process is more evident in those samples with higher Fe content, specifically for x = 0.20 and 0.06.

DSC scans recorded at 20 K/min from room temperature to 973 K for samples milled 50 h are presented in **Fig. 2**. In all samples, exothermic transformation processes are observed ascribed to the crystallization of the amorphous phase developed during milling. **Table 2** shows parameters from DSC scans, such as peak temperatures and heat of transformation. XRD patterns of 50 h milled samples heated up to 723 K at 20 K/min in the calorimeter (**Fig. 3**) show that, independently of Fe content, the stable and single-phase formed is the hexagonal austenite intermetallic MnCoGe-type ($P6_3/mmc$ space group). There are some differences in relation to crystal size: the sample with highest Fe content shows D = 14.1 ± 0.3 nm, while other samples show similar values, D = 17.2 ± 0.2 and 17.1 ± 0.2 nm, for x = 0.06 and 0.03 respectively.

Table 2. Parameters from DSC scans

Fe content	**x = 0.20**	**x = 0.06**			**x = 0.03**	
Peak temperature (K)	562	576	634	873	576	634
Transformation heat (J/g)	52 ± 1	63 ± 1		6 ± 1	66 ± 1	

J. Alloys and Compounds 930 (2023) 167381 1D
https://doi.org/10.1016/j.jallcom.2022.167381

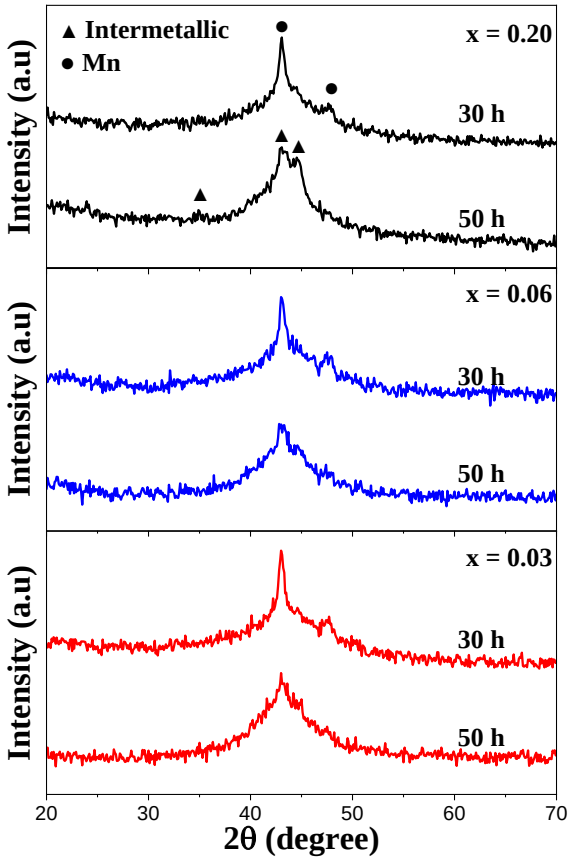

Fig. 1. Room temperature XRD patterns of mechanically alloyed $MnCo_{1-x}Fe_xGe$ after 30 and 50 h milling, where x = 0.20 (black), x = 0.06 (blue) and x = 0.03 (red).

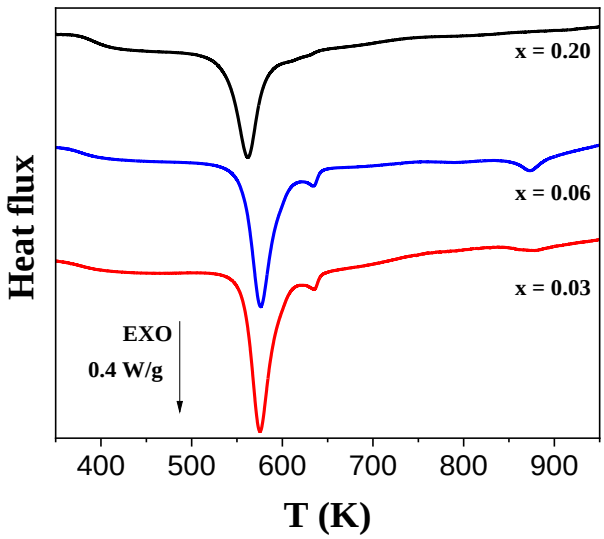

Fig. 2. DSC scans at 20 K/min from room temperature to 973 K for $MnCo_{1-x}Fe_xGe$ samples milled for 50h (x = 0.20, 0.06 and 0.03).The arrow indicates the magnitude and nature of the transformations; in this case, all of them are exothermic transformations.

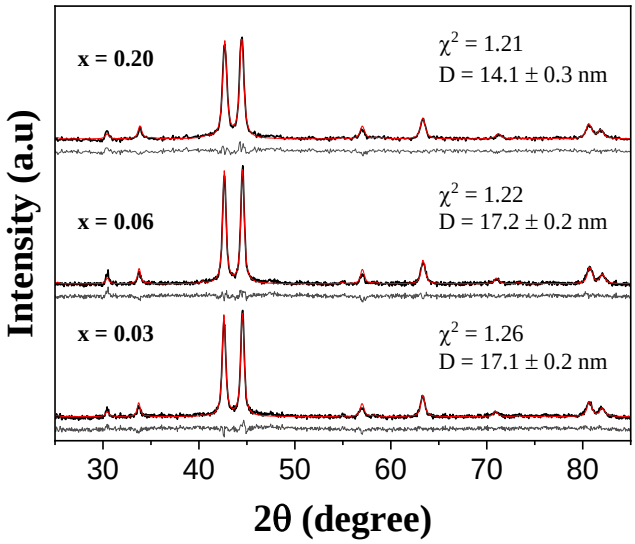

Fig. 3. Room temperature XRD patterns of $MnCo_{1-x}Fe_xGe$ samples milled for 50 h and then heated up to 723 K at 20 K/min in the calorimeter. The experimental data are shown in black, and the Rietveld fittings are shown in red The corresponding differences between the experimental data and the Rietveld fittings are shown below each experimental pattern. **D** indicates the crystal size and χ^2 indicates the goodness of fit.

Fig. 4 shows in situ XRD patterns of the different studied samples as a function of temperature (between 150 and 450 K). All samples show the austenite intermetallic as a single phase in all the temperature studied range.

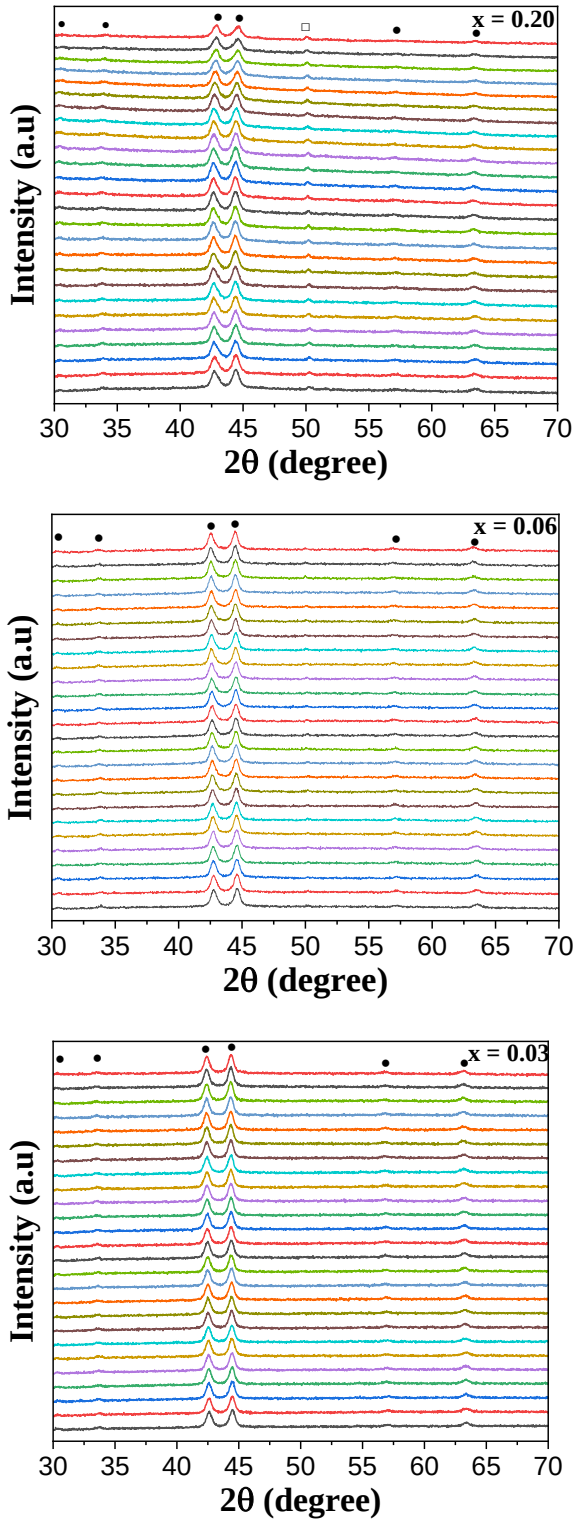

Fig. 4. XRD patterns as a function of temperature (from 150, upper curve, to 400 K, lower curve, every 10 K) of $MnCo_{1-x}Fe_xGe$ samples milled for 50 h and then heated up to 723 K at 20 K/min in the calorimeter. Solid circles correspond to the hexagonal phase (austenite) and the hollow square at x = 0.20 corresponds to the sample holder.

XRD results were analyzed by Rietveld fitting (goodness of fit below 1.3). **Fig. 5** shows the temperature evolution of lattice parameters, a and c, of the intermetallic phase. For x = 0.06, both lattice parameters linearly increase with temperature as a result of regular thermal expansion. This behavior is also found for x = 0.03, but some deviations appear at high temperature. However, for x = 0.20, the lattice parameters do not present that simple behavior and they can even decrease with temperature [22]. **Fig. 6** shows the temperature evolution of cell volume.

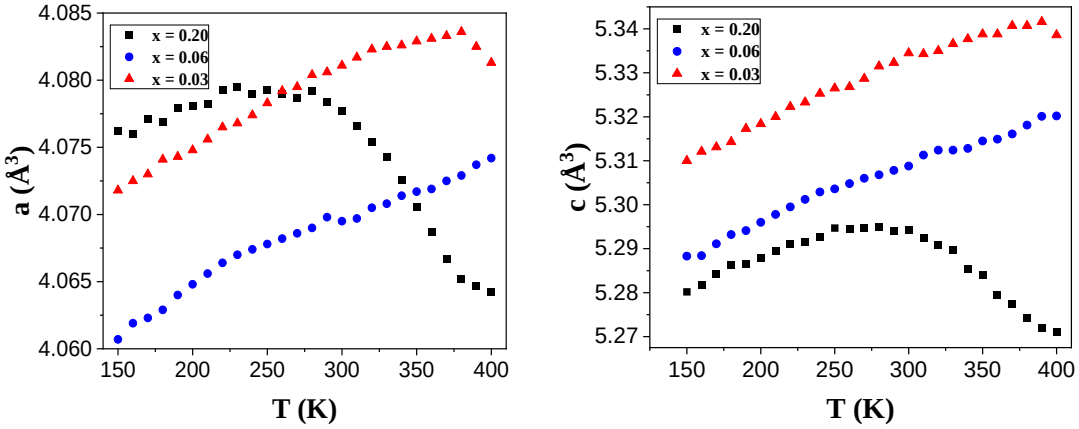

Fig. 5. Evolution as a function of temperature of lattice parameters, a and c, of the intermetallic phase detected by XRD.

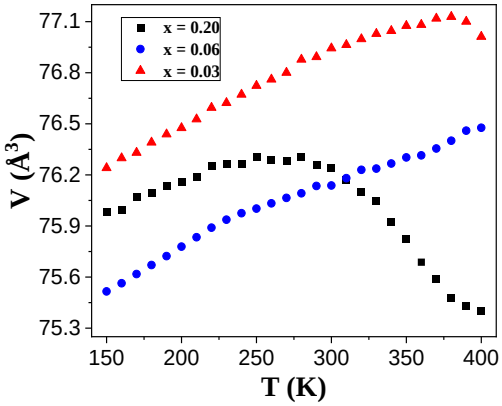

Fig. 6. Evolution of cell volume of the intermetallic phase detected by XRD as a function of temperature.

Concerning magnetic properties, isothermal specific magnetization curves ($\sigma(T,H)$) are shown in **Fig. 7** as a function of Fe content for samples milled 50 h and then heated up to 723 K at 20 K/min. Magnetization decreases as temperature approaches that of the magnetic transition from the ferromagnetic to the paramagnetic state. From the $\sigma(T,H)$ data, ΔS_m was obtained and **Fig.** 8 shows the magnetic entropy change for a

maximum field change $\mu_0\Delta H = 1.5$ T as a function of Fe content and **Table 3** collects the main MCE parameters including refrigerant capacity defined as $RC_{FWHM} = \Delta S_M^{peak} \cdot \Delta T$, where ΔT is the full width at half maximum of MCE peak. As Fe content decreases, $|\Delta S_M|$ slightly increases. However, there is no monotonous trend in T_c and sample with x = 0.06 shows a slightly higher Curie temperature than the other two samples.

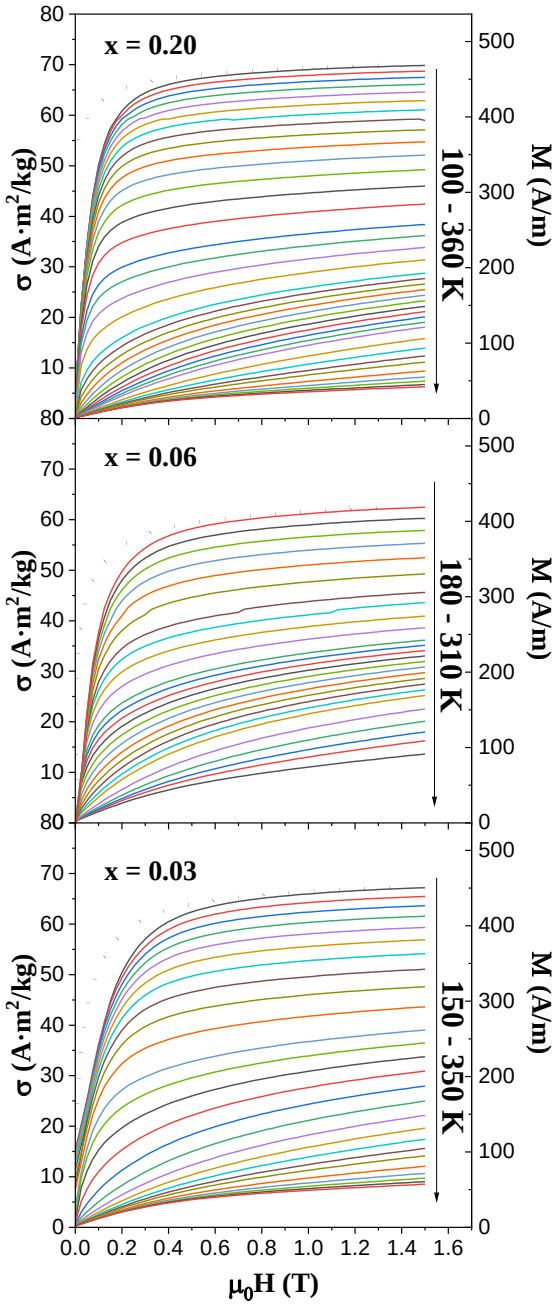

Fig. 7. Isothermal magnetization curves as a function of Fe content for samples milled 50 h and then heated up to 723 K at 20 K/min. Dotted curves correspond to magnetization curves at the lower temperatures corrected from the demagnetizing field (assuming *N*=0.25). Arrows indicate the evolution of temperature in the indicated range. A density of 6707 kg/m^3 has been used to obtain magnetization M from σ data. Temperature range, ΔT = 10 K between 100-240 K , 300-350 K , ΔT = 5 K between 240-260 K, 280-300 K and ΔT = 2 K between 260-280 K.

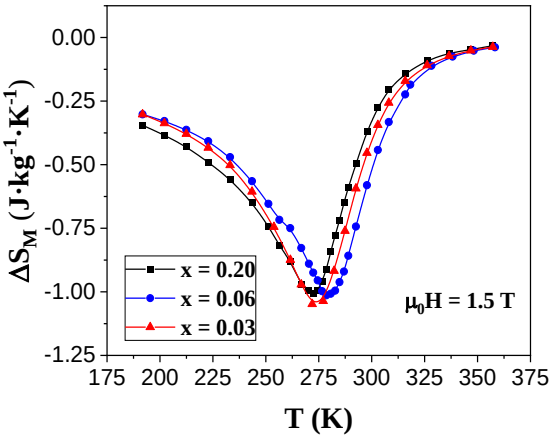

Fig. 8. Temperature dependence of ΔS_M as a function of Fe content for samples milled for 50 h and then heated up to 723 K at 20 K/min in the calorimeter. Black squares correspond to samples with x = 0.20, blue circles correspond to samples with x = 0.06, and red triangles correspond to samples with x = 0.03.

Table 3. MCE response at $\mu_0\Delta H$ = 1.5 T as a function of Fe content

Fe content	Max ΔS_M ± 0.01 (J·kg^{-1}·K^{-1})	RC_{FWHM} ± 3 (J·kg^{-1})	T_C ± 3 (K)
0.20	-1.01	-66	272
0.06	-1.02	-62	279
0.03	-1.05	-61	275

4. Discussion

Recently, Manchón-Gordón et al. proposed a method to obtain the parameters of a gaussian distribution of T_C (average value $\langle T_C \rangle$ and standard deviation ΔT_c), based on the Weiss model [23,24]. This method uses the dependence on $\langle T_C \rangle$ and ΔT_c of the inflexion point temperature, T_{inf}, of the saturation magnetization at zero field, $M_s(T)$, and the peak temperature, T_χ, of the paramagnetic susceptibility (χ_p), which can be obtained from the linear fitting of the law of approach to saturation of the $M(T,H)$ curves. This law can be simplified to: $M = M_S + \chi_p H$ where H is the internal field (magnetic fields above 1 T are taken, so the effects of demagnetizing factor are negligible). Effects involved by structural inhomogeneities caused by defects within magnetic substances and effective anisotropy have not been considered. Additionally, the peak temperature of the MCE, T_{MCE}, also depends on $\langle T_C \rangle$ and ΔT_c. The following equations [25] describe such dependences:

$$T_{inf}^{Weiss} - \langle T_C \rangle = -0.732(6)\Delta T_c \quad (2)$$

$$T_{MCE}^{Weiss} - \langle T_C \rangle = -0.658(8)\Delta T_c \quad (3)$$

$$T_{\chi}^{Weiss} - \langle T_C \rangle = 0.503(24)\Delta T_c - 0.0040(7)\Delta T_C^2 \quad (4)$$

Where superscript Weiss indicates the use of this model to describe the magnetization.

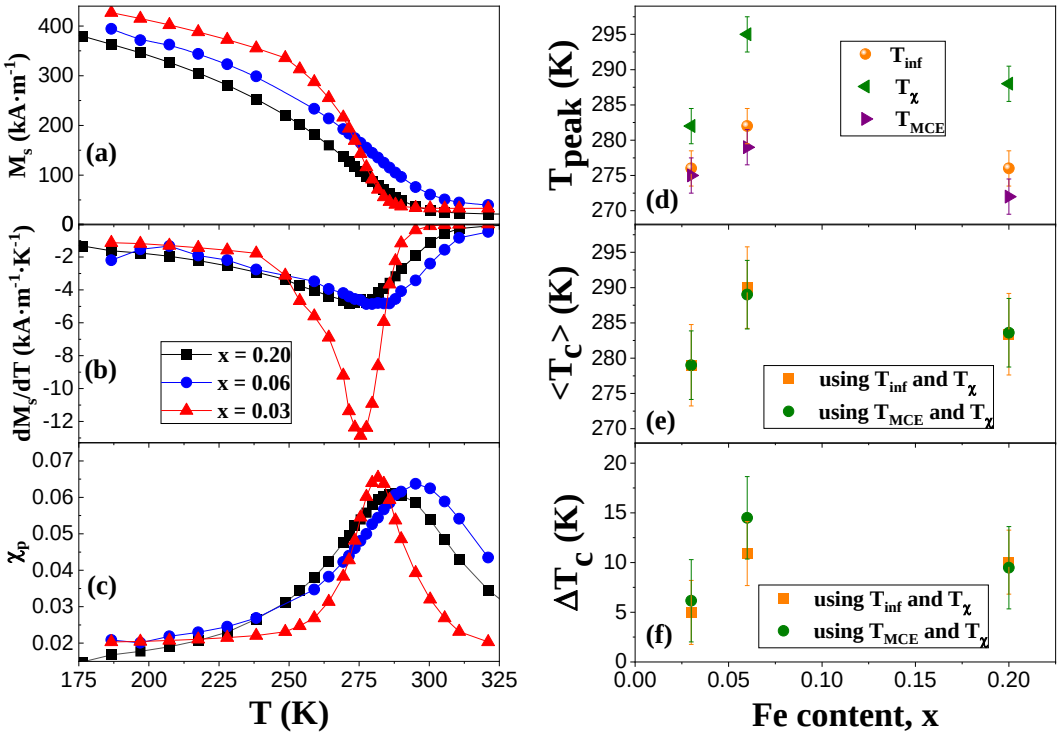

Fig. 9. (a) Experimental data for M_S, **(b)** dM_S/dT , **(c)** χ_P curves from the analysis of approach to saturation for $MnCo_{1-x}Fe_xGe$ samples milled for 50 h and then heated up 723 K at 20 K/min in the calorimeter. **(d)** Experimental peak temperatures for: dM_S/dT, χ_P and $\Delta S_M(T)$ curves; **(e)** mean Curie temperatures, $\langle T_C \rangle$; and **(f)** standard deviation, ΔT_C, of the distribution of transition temperatures from Equations (2), (3) and (4), as a function of iron content.

Fig. 9 **a**, **b** and **c** show, for the different studied compositions, the experimental data of M_S, dM_S/dT and χ_p from the analysis of approach to saturation (using a density of 6707 kg/m^3). It can be seen how magnetization does not go to zero in the paramagnetic range. This may be due to the presence of ferromagnetic inhomogeneities. This remaining value of magnetization should correspond to 1% volume of magnetic impurities (using magnetic moment of iron).

Fig. 9 d shows the different experimental peak temperatures used in equations (2)-(4). Results for $\langle T_C \rangle$ and ΔT_c are shown in **Fig. 9 e** and **f**, respectively. Despite the large error, the estimated broadenings are 5, 12 and 10 K for x = 0.03, 0.06 and 0.2, respectively. These values are in agreement with the expected increase of the n exponent due to the presence of a Curie temperature distribution [26]. The out of equilibrium method of sample production leading to this distribution can also explain that austenite phase stabilizes in our samples unlike results reported from other authors for similar compositions produced by arc-melting, where martensite phase is found [12]. In our study, mechanical alloying stabilizes the phase with higher entropy. **Fig.** 10 shows the magnetic transition temperatures obtained in our study along with the results from Li et al. [12].

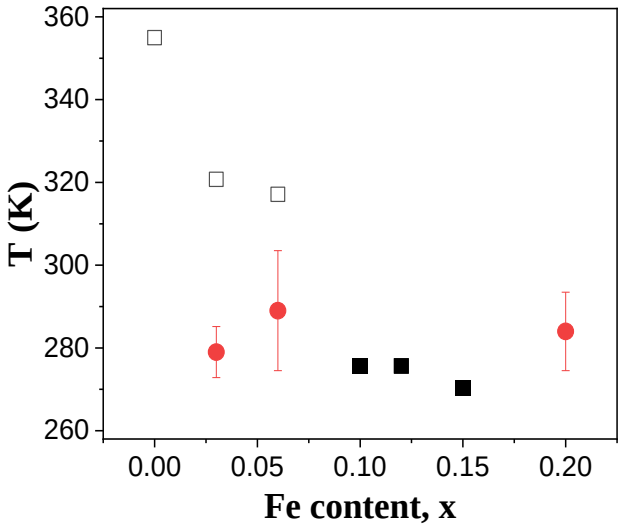

Fig. 10. Magnetic transformation temperatures as a function of Fe content. Hollow symbols correspond to martensite phase and full symbols to austenite phase. Squares are taken from [12] and circles are measurements from this work (average values from Weiss distribution are represented and error bars correspond to the standard deviation of the distribution).

This analysis evidences the presence of a distribution which is a fact worth it taking into account when discussing the order character of the transition. The nature of the observed magnetic transition can be studied using the Banerjee criterion [27] which indicates that the slopes of the isotherms in the Arrot plots (H/M versus M^2) must be negative in the case of a FOPT, whereas positive slopes are indicative of a SOPT.

Fig. 11 shows the Arrot plots corresponding to the data shown in **Fig.** 7 . Therefore, according to Banerjee criterion, these samples should exhibit SOPT. However, recent results showed that there are other criteria that allow evaluating the order of the phase transition based on the field exponent of the magnetic entropy change [28], which can identify more precisely the order of the transition.

The field dependence of the magnetic entropy change is represented as a power law of the field, $\Delta S_M \propto H^n$, with a n exponent that, in general, is field and temperature dependent [29]. In the paramagnetic range, magnetization behaves according to the Curie-Weiss law, which leads to n = 2. In the ferromagnetic range and well below the transition, n = 1. Finally, at the transition temperature, T_c, for SOPTs, the n exponent is related to the critical exponents of the material:

$$n(T_C) = 1 + \frac{1}{\delta}\left(1 - \frac{1}{\beta}\right) \quad (5)$$

Where β and δ are critical exponents which can be related to a third critical exponent, γ: $\delta = 1 + \gamma/\beta$.

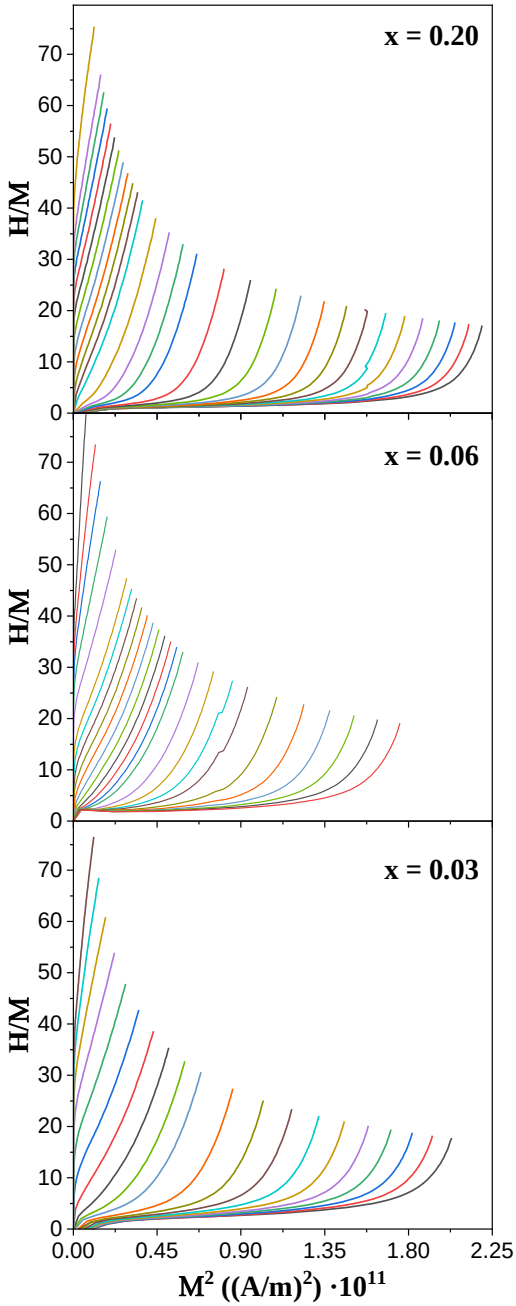

Fig. 11. Arrot plots as a function of Fe content for samples milled 50 h and then heated up to 723 K at 20 K/min.

Moreover, the behavior of n during the transition can be used as a footprint of the transition order. In fact, on the one hand, for second order phase transitions, at temperatures above the transition n approaches to n = 2 from lower values. On the other hand, in first order phase transitions, n reaches values > 2 for temperatures above the transition [28]. Despite, the presence of a distribution can smooth this peak, values above 2 are preserved (as finally, at higher temperatures of the distribution, average might be obtained from values ≥ 2), being an evidence of the presence of a first order character in the transition.

Non-negligible effects of the demagnetizing factor, N [30] makes necessary to correct the magnetization curves from the demagnetizing field using the internal field, $H = H_{ap} - NM$, instead of the applied field H_{ap} (a density of 6707 kg/m^3 has been used to obtain magnetization M from σ data). This was done with the aim to compare our results to the predictions of theoretical analyses that show that the field exponent n of magnetic entropy change presents a maximum of $n > 2$ only for first-order thermomagnetic phase transitions [28]. **Fig.** 12 shows the experimentally determined n exponent as a function of temperature for the different compositions for a maximum magnetic field change of 1 T for uncorrected (using H_{ap} and represented as solid symbols) and corrected (using $H = H_{ap} - NM$ and represented as hollow symbols) curves of $M(T, H)$ assuming $N \sim 0.25$ (estimated from the deviation of n exponent for $T << T_C$ [31]).

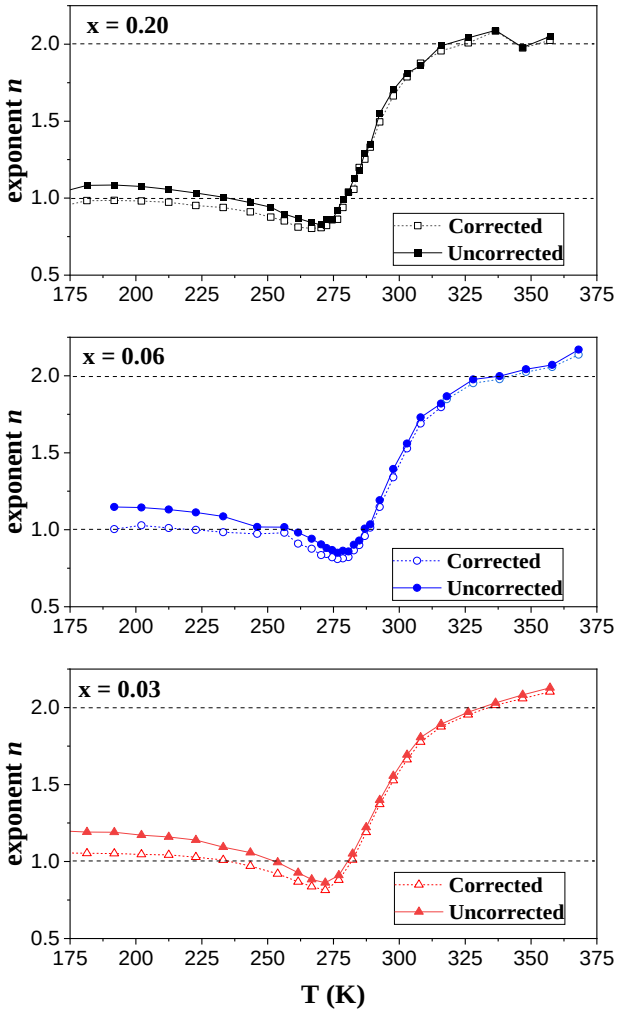

Fig. 12. Experimental *n*(T) curves as a function of Fe content for samples milled for 50 h and then heated up to 723 K at 20 K/min in the calorimeter for 1.0 T of applied field (uncorrected curves, solids symbols) or internal field (corrected curves using N = 0.25, hollow symbols).

Once considering the demagnetizing factor, the values of n at $T << T_C$ recover the expected value close to one. However, at T_C values are clearly higher than the expected ones: $n^{peak} = 0.80$, 0.81 and 0.81 for x = 0.20, 0.06 and 0.03, respectively, instead of $n^{peak} \sim 0.67$ for a mean field SOPT [29]. This fact can be due to the existence of inhomogeneities which can lead to the existence of a broad T_C distribution in these samples. Comparison between the mean field value for pure phase, $n^{peak} \sim 0.67$, and the obtained ones should lead to values of the distribution width around 10 K [26]. The source of this distribution could be compositional as it is known that T_C can be tailored in these compositions by changing the Fe content [10,32].

This fact supports the characteristic corresponding to FOPT inferred from the behavior of the field n exponent but does not agree with Arrott-plot (see **Fig. 11**). Certainly, there is a considerable volume variation without modification of the crystal structure (i.e. a magnetoelastic transition) as shown in **Fig. 6**. However, the presence of a distribution of Curie temperatures in the samples may jeopardize the weak FOPT character, in fact second order behavior prevails over first order contributions in Arrott-plots when the response of a mixture of phases is analyzed [33–36].

5. Conclusions

Mechanical alloying allows us to produce precursor amorphous Mn(Co,Fe)Ge alloys which, after annealing, develop the hexagonal austenite phase. Despite, martensitic transformation to lower entropy orthorhombic phase is not detected, magnetic transition of higher entropy hexagonal phase shows interesting magnetocaloric properties.

However, the character of the transition is not straightforward. On the one hand, according to Banerjee's criterion, the transition should be second-order. However, this interpretation must be affected by the presence of a distribution of transition temperatures. On the other hand, analysis of the field dependence of ΔS_m states that the transition should be first-order, which is verified by detecting a cell volume variation, and thus a magnetoelastic transition, clearer for the sample with the highest Fe content.

CRediT authorship contribution statement

A. Vidal-Crespo: Conceptualization, Formal analysis, Investigation, Writing - original draft. **J.J. Ipus**: Conceptualization, Methodology, Investigation, Resources, Writing - review & editing. **J.S. Blázquez**: Conceptualization, Methodology, Investigation, Resources, Writing - review & editing, Supervision. **C. F. Conde**: Methodology, Resources, Writing - review & editing, Supervision**.**

Declaration of Competing Interest

The authors declare that they have no known competing financial interest or personal relationships that could have appeared to influence the work reported in this paper.

Acknowledgments

This work was supported by AEI/FEDER-UE (Projects US-1260179), the PAI of the Regional Government of Andalucía (P18-RT-746), and the VI-PPITU from Universidad de Sevilla (Spain). A. Vidal-Crespo acknowledges the financial support of the VI-PPITU from Universidad de Sevilla (Spain).

References

1. Kitanovski, A.; Tušek, J.; Tomc, U.; Plaznik, U.; Ožbolt, M.; Poredoš, A. *Magnetocaloric Energy Conversion*; Springer International Publishing: Cham, 2015; ISBN 9783319087405 9783319087412.
2. Franco, V.; Blázquez, J.S.; Ipus, J.J.; Law, J.Y.; Moreno-Ramírez, L.M.; Conde, A. Magnetocaloric effect: From materials research to refrigeration devices. *Prog. Mater. Sci.* **2018**, *93*, 112–232, doi:https://doi.org/10.1016/j.pmatsci.2017.10.005.
3. Gutfleisch, O.; Willard, M.A.; Brück, E.; Chen, C.H.; Sankar, S.G.; Liu, J.P. Magnetic Materials and Devices for the 21st Century: Stronger, Lighter, and More Energy Efficient. *Adv. Mater.* **2011**, *23*, 821–842, doi:10.1002/adma.201002180.
4. Wang, C.C.; Hu, Q.B.; Zhang, L.; Wei, M.Z. The investigation of magnetic phase transitions and magnetocaloric properties in high-pressure annealed MnNiFeGe alloy. *Philos. Mag.* **2021**, *101*, 964–975, doi:10.1080/14786435.2021.1873450.
5. Marchenkov, V. V; Emelyanova, S.M. Low-temperature hall effect and martensitic transition temperatures in magnetocaloric Ni50Mn35Sb15-xGex (x=0, 1, 3) alloys. *LOW Temp. Phys.* **2021**, *47*, 55–60, doi:10.1063/10.0002898.
6. Sasmaz, M. Metamagnetic transition and magnetocaloric properties of Ni45Mn42In13 Heusler alloy. *PHASE TRANSITIONS* **2021**, *94*, 289–297, doi:10.1080/01411594.2021.1931691.
7. Mao, Y.W.; Zhang, C.C.; Wang, R.L.; Xiao, H.B.; Xu, L.F.; Xia, Z.C.; Yang, C.P. Large successive magnetocaloric effects around room temperature in Ni50Mn34In15Al alloy. *Eur. Phys. J. B* **2018**, *91*, doi:10.1140/epjb/e2018-80721-9.
8. Bao, L.F.; Huang, W.D.; Ren, Y.J. Tuning Martensitic Phase Transition by Non-Magnetic Atom Vacancy in MnCoGe Alloys and Related Giant Magnetocaloric Effect. *CHINESE Phys. Lett.* **2016**, *33*, doi:10.1088/0256-307X/33/7/077502.

9. Krenke, T.; Duman, E.; Acet, M.; Wassermann, E.F.; Moya, X.; Mañosa, L.; Planes, A. Inverse magnetocaloric effect in ferromagnetic Ni–Mn–Sn alloys. *Nat. Mater.* **2005**, *4*, 450–454, doi:10.1038/nmat1395.

10. Li, G.J.; Liu, E.K.; Zhang, H.G.; Zhang, Y.J.; Chen, J.L.; Wang, W.H.; Zhang, H.W.; Wu, G.H.; Yu, S.Y. Phase diagram, ferromagnetic martensitic transformation and magnetoresponsive properties of Fe-doped MnCoGe alloys. *J. Magn. Magn. Mater.* **2013**, *332*, 146–150, doi:https://doi.org/10.1016/j.jmmm.2012.12.001.

11. Jeitschko, W. A high-temperature X-ray study of the displacive phase transition in MnCoGe. *Acta Crystallogr. Sect. B Struct. Crystallogr. Cryst. Chem.* **1975**, *31*, 1187–1190, doi:10.1107/s0567740875004773.

12. Li, G.J.; Liu, E.K.; Zhang, H.G.; Zhang, Y.J.; Chen, J.L.; Wang, W.H.; Zhang, H.W.; Wu, G.H.; Yu, S.Y. Phase diagram, ferromagnetic martensitic transformation and magnetoresponsive properties of Fe-doped MnCoGe alloys. *J. Magn. Magn. Mater.* **2013**, *332*, 146–150, doi:10.1016/j.jmmm.2012.12.001.

13. Ozono, K.; Mitsui, Y.; Umetsu, R.Y.; Hiroi, M.; Takahashi, K.; Koyama, K. Magnetic and structural properties of MnCo1-xFexGe ($0 \leq x \leq 0.12$). *AIP Conf. Proc.* **2016**, *1763*, 20003, doi:10.1063/1.4961336.

14. Lin, S.; Tegus, O.; Bruck, E.; Dagula, W.; Gortenmulder, T.J.; Buschow, K.H.J. Structural and Magnetic Properties of MnFe1-xCoxGe Compounds. *IEEE Trans. Magn.* **2006**, *42*, 3776–3778, doi:10.1109/TMAG.2006.884516.

15. Rahman, A.R.; Md Din, M.F.; Wang, J.; Suhaimi, N.S.; Idris, N.H.; Dou, S.X.; Ismail, M.; Hassan, M.Z.; Jusoh, M.T. Magnetism and Thermomechanical Properties in Si Substituted MnCoGe Compounds. *Cryst.* 2021, *11*.

16. Bi, Y.; He, W.; Yang, T.; Wu, W.; Wen, J.; Yu, X.; Chen, F. The Effects of La Doping on the Crystal Structure and Magnetic Properties of Ni2In-Type MnCoGe1−xLax (x = 0, 0.01, 0.03) Alloys. *Mater.* 2021, *14*.

17. Song, Y.; Ma, S.; Yang, F.; Zhang, Z.; Zhang, Y.; Zeng, H.; Ur Rehman, S.; Feng, G.; Luo, X.; Chen, C.; et al. Co-vacancy induced magneto-structural transformation in Co and Ge bidirectional-regulation MnCoGe systems. *J. Alloys Compd.* **2020**, *819*, 153061, doi:https://doi.org/10.1016/j.jallcom.2019.153061.

18. Suryanarayana, C. Mechanical alloying and milling. *Prog. Mater. Sci.* **2001**, *46*, 1–184, doi:https://doi.org/10.1016/S0079-6425(99)00010-9.

19. Vidal-Crespo, A.; Ipus, J.J.; Blázquez, J.S.; Conde, A. Obtaining magnetocaloric MnCo(Fe)Ge intermetallics from low temperature treatment of mechanically alloyed precursors. *J. Magn. Magn. Mater.* **2020**, *514*, 167127, doi:https://doi.org/10.1016/j.jmmm.2020.167127.

20. Vidal-Crespo, A.; Ipus, J.J.; Blázquez, J.S.; Conde, A. Mechanical Amorphization and Recrystallization of Mn-Co(Fe)-Ge(Si) Compositions. *Metals (Basel).* **2019**, *9*, 534, doi:10.3390/met9050534.

21. Franco, V. Determination of the Magnetic Entropy Change from Magnetic Measurements : the Importance of the Measurement Protocol. **2014**, 1–19.

22. Zhao, Y.-Y.; Hu, F.-X.; Bao, L.-F.; Wang, J.; Wu, H.; Huang, Q.-Z.; Wu, R.-R.;

Liu, Y.; Shen, F.-R.; Kuang, H.; et al. Giant Negative Thermal Expansion in Bonded MnCoGe-Based Compounds with Ni2In-Type Hexagonal Structure. *J. Am. Chem. Soc.* **2015**, *137*, 1746–1749, doi:10.1021/ja510693a.

23. Manchón-Gordón, A.F.; Moreno-Ramírez, L.M.; Ipus, J.J.; Blázquez, J.S.; Conde, C.F.; Franco, V.; Conde, A. A procedure to obtain the parameters of Curie temperature distribution from thermomagnetic and magnetocaloric data. *J. Non. Cryst. Solids* **2019**, *520*, 119460, doi:https://doi.org/10.1016/j.jnoncrysol.2019.119460.

24. Manchón-Gordón, A.F.; Moreno-Ramírez, L.M.; Ipus, J.J.; Blázquez, J.S.; Conde, C.F.; Franco, V.; Conde, A. Correction to "A procedure to obtain the parameters of curie temperature distribution from thermomagnetic and magnetocaloric data" orginally published as J. non-cryst. solids 520, 119,460 (2019). *J. Non. Cryst. Solids* **2020**, *538*, 120047, doi:https://doi.org/10.1016/j.jnoncrysol.2020.120047.

25. Manchón-Gordón, A.F.; López-Martín, R.; Vidal-Crespo, A.; Ipus, J.J.; Blázquez, J.S.; Conde, C.F.; Conde, A. Distribution of Transition Temperatures in Magnetic Transformations: Sources, Effects and Procedures to Extract Information from Experimental Data. *Metals (Basel).* **2020**, *10*, 226, doi:10.3390/met10020226.

26. Doblas, D.; Moreno-Ramírez, L.M.; Franco, V.; Conde, A.; Svalov, A. V; Kurlyandskaya, G. V Nanostructuring as a procedure to control the field dependence of the magnetocaloric effect. *Mater. Des.* **2017**, *114*, 214–219, doi:https://doi.org/10.1016/j.matdes.2016.11.085.

27. Banerjee, B.K. On a generalised approach to first and second order magnetic transitions. *Phys. Lett.* **1964**, *12*, 16–17, doi:10.1016/0031-9163(64)91158-8.

28. Law, J.Y.; Franco, V.; Moreno-Ramírez, L.M.; Conde, A.; Karpenkov, D.Y.; Radulov, I.; Skokov, K.P.; Gutfleisch, O. A quantitative criterion for determining the order of magnetic phase transitions using the magnetocaloric effect. *Nat. Commun.* **2018**, *9*, 2680, doi:10.1038/s41467-018-05111-w.

29. Franco, V.; Blázquez, J.S.; Conde, A. Field dependence of the magnetocaloric effect in materials with a second order phase transition: A master curve for the magnetic entropy change. *Appl. Phys. Lett.* **2006**, *89*, 9–12, doi:10.1063/1.2399361.

30. Caballero-Flores, R.; Franco, V.; Conde, A.; Kiss, L.F. Influence of the demagnetizing field on the determination of the magnetocaloric effect from magnetization curves. *J. Appl. Phys.* **2009**, *105*, 07A919, doi:10.1063/1.3067463.

31. Romero-Muñiz, C.; Ipus, J.J.; Blázquez, J.S.; Franco, V.; Conde, A. Influence of the demagnetizing factor on the magnetocaloric effect: Critical scaling and numerical simulations. *Appl. Phys. Lett.* **2014**, *104*, 252405, doi:10.1063/1.4885110.

32. Johnson, V. Diffusionless orthorhombic to hexagonal transitions in ternary silicides and germanides. *Inorg. Chem.* **1975**, *14*, 1117–1120, doi:10.1021/ic50147a032.

33. Moreno-Ramírez, L.M.; Romero-Muñiz, C.; Law, J.Y.; Franco, V.; Conde, A.;

Radulov, I.A.; Maccari, F.; Skokov, K.P.; Gutfleisch, O. Tunable first order transition in La(Fe,Cr,Si)13 compounds: Retaining magnetocaloric response despite a magnetic moment reduction. *Acta Mater.* **2019**, *175*, 406–414, doi:https://doi.org/10.1016/j.actamat.2019.06.022.

34. Bustingorry, S.; Pomiro, F.; Aurelio, G.; Curiale, J. Second-order magnetic critical points at finite magnetic fields: Revisiting Arrott plots. *Phys. Rev. B* **2016**, *93*, 224429, doi:10.1103/PhysRevB.93.224429.

35. Bonilla, C.M.; Herrero-Albillos, J.; Bartolomé, F.; García, L.M.; Parra-Borderías, M.; Franco, V. Universal behavior for magnetic entropy change in magnetocaloric materials: An analysis on the nature of phase transitions. *Phys. Rev. B* **2010**, *81*, 224424, doi:10.1103/PhysRevB.81.224424.

36. Sánchez-Pérez, M.; Moreno-Ramírez, L.M.; Franco, V.; Conde, A.; Marsilius, M.; Herzer, G. Influence of nanocrystallization on the magnetocaloric properties of Ni-based amorphous alloys: Determination of critical exponents in multiphase systems. *J. Alloys Compd.* **2016**, *686*, 717–722, doi:https://doi.org/10.1016/j.jallcom.2016.06.057.